Reconfigurable Hexapartite Entanglement by Spatially Multiplexed Four-Wave Mixing Processes

Kai Zhang,[1] Wei Wang,[1] Shengshuai Liu,[1] Xiaozhou Pan,[1] Jinjian Du,[1] Yanbo Lou,[1] Sheng Yu,[1] Shuchao Lv,[1] Nicolas Treps,[2,*] Claude Fabre,[2,†] and Jietai Jing[1,3,4,‡]

[1]*State Key Laboratory of Precision Spectroscopy, Joint Institute of Advanced Science and Technology, School of Physics and Electronic Science, East China Normal University, Shanghai 200062, China*

[2]*Laboratoire Kastler Brossel, Sorbonne Université, CNRS, ENS-PSL Research University, Collège de France, 4 place Jussieu, 75252 Paris, France*

[3]*Department of Physics, Zhejiang University, Hangzhou 310027, China*

[4]*Collaborative Innovation Center of Extreme Optics, Shanxi University, Taiyuan, Shanxi 030006, China*

(Received 17 July 2019; accepted 28 January 2020; published 3 March 2020)

Multipartite entanglement serves as a vital resource for quantum information processing. Generally, its generation requires complex beam splitting processes which limit scalability. A promising trend is to integrate multiple nonlinear processes into a single device via frequency or time multiplexing. The generated states in these schemes are useful for quantum computation. However, they are confined in one or two beams and hard to be spatially separated for applications in quantum communication. Here, we experimentally demonstrate a scheme to generate spatially separated hexapartite entangled states by means of spatially multiplexing seven concurrent four-wave mixing processes. In addition, we show that the entanglement structure characterized by subsystem entanglement distribution can be modified by appropriately shaping the pump characteristics. Such reconfigurability of the entanglement structure gives the possibility to target a desired multipartite entangled state for a specific quantum communication protocol. Our results here provide a new platform for generating large scale spatially separated reconfigurable multipartite entangled beams.

DOI: 10.1103/PhysRevLett.124.090501

Multipartite entanglement plays a crucial role not only in the field of testing fundamental quantum effects [1] but also in the applications to quantum communication [2,3] and quantum computation [4,5]. There have been numerous demonstrations both in continuous-variable (CV) [6–9] and discrete-variable (DV) regimes [10,11]. Conventionally, these implementations involve complex linear [6–10] or nonlinear [11] successive beam splitting processes. Therefore, the complexity of such an experimental layout increases dramatically with the increase of the mode number of the generated entangled state.

To circumvent these inherent defects, previous attempts in the CV regime have been focused on integrating multiple nonlinear processes into a single device using frequency multiplexing [12–15] and time multiplexing [16]. These schemes are undoubtedly beneficial to quantum computation. However, they are not suitable for conveying the quantum information among different locations since the generated beams are usually confined in one or two beams. Therefore, a scalable scheme able to generate spatially separated entangled beams is essential for building distant quantum communication networks. In this respect, a novel method with good scalability utilizing a spatially structured pump (SSP) to generate spatially separated entangled beams has been theoretically proposed [17,18]. This method is in fact related to the concept of spatial multiplexing [19–21]. It enables both the enhancement of scalability and natural separation of light beams. Furthermore, the structure of the quantum network is governed by the shape of the SSP. It can then be tailored by pump shaping techniques. This is necessary for quantum information protocols, as for a given application, a given entanglement structure is required.

The four-wave mixing (FWM) process in a hot atomic vapor cell has been shown as a promising and simple resource for both quantum information [22–26] and quantum metrology [27] due to its advantages for practical implementations, e.g., no need for a cavity and spatial separation of the generated nonclassical beams. Therefore, it could be a good candidate for producing CV multipartite entanglement although currently such a system has only been used to generate bipartite entanglement [22,23]. In this Letter, we experimentally generate hexapartite entanglement by spatially multiplexing seven concurrent FWM processes. Such multiplexing is enabled by using a SSP that consists of two strong intersecting pump beams. More interestingly, we find that the structure of the hexapartite entanglement characterized by subsystem entanglement distribution can be easily reconfigured by regulating the power ratio of the two strong pump beams, i.e., pump shaping. Several works [28–31] also involve dual-pump

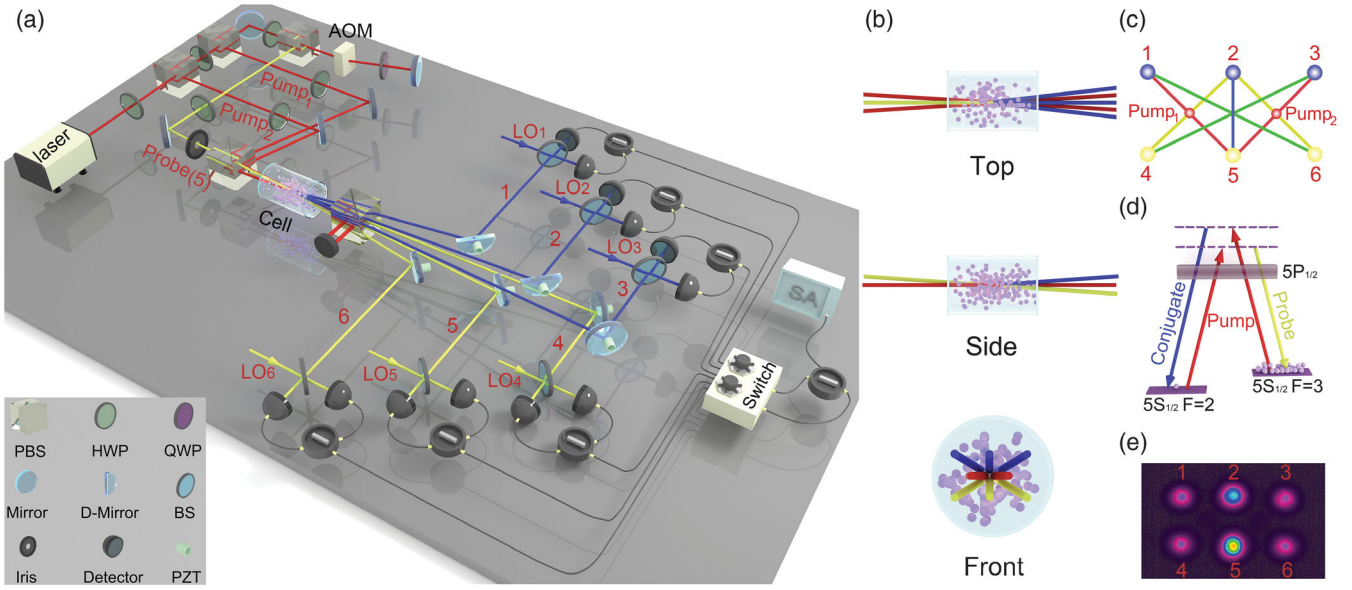

FIG. 1. Schematic of hexapartite entanglement generation and detection. (a) Experimental setup. Acousto-optic modulator (AOM), polarization beam splitter (PBS), half wave plate (HWP), quarter wave plate (QWP), high reflectivity mirror (Mirror), D-shaped mirror (D-Mirror), beam splitter (BS), piezo-electric transducer (PZT), two home-made single pole six-throw switches (Switch), spectrum analyzer (SA). (b) The input and output beams configuration from the top, side, and front views, respectively. (c) Transverse distribution of the different beams exiting from the cell. (d) Double-lambda energy level sketch of the FWM process. (e) The camera-captured two-dimensional intensity pattern of the output fields when the probe beam 5 is on.

schemes and study the intensity correlation properties of the generated fields. Here we fully characterize the generated multimode state by measuring the full multipartite covariance matrix and show in particular multipartite entanglement and the pump shaping effect on manipulation of multipartite entanglement.

The experimental setup for generation and detection of the hexapartite entanglement is shown in Fig. 1(a). From a Ti:sapphire laser tuned about 0.85 GHz to the blue of the ^{85}Rb D1 line transition ($5S_{1/2} \rightarrow 5P_{1/2}$), two pump beams of adjustable powers (Pump_1 and Pump_2) are generated. They intersect at an angle of 8 mrad in the center of a 12 mm long ^{85}Rb vapor cell heated at 118 °C, and form the SSP. The probe beam (5), 3.04 GHz redshifted from the pump beams, is generated by sending part of the pump beam double passing through an acousto-optic modulator and is symmetrically crossed with the two pump beams at an angle of about 5.7 mrad, resulting in the natural spatial separation of the output beams. The waists of the individual pump beam and probe beam are 605 and 303 μm, respectively. To better illustrate the spatial distribution of the input and output beams, we depict the configuration of the involved beams from the top, side, and front views, respectively, as shown in Fig. 1(b). Under this configuration, seven FWM processes can be spatially multiplexed in the same vapor cell as shown in Fig. 1(c). First of all, the probe beam (5) can interact with each pump beam via the normal single-pump FWM process. The probe beam is amplified and two conjugate beams (1 and 3) are simultaneously generated [these two FWM interactions are indicated by the red straight lines connecting the relevant beams in Fig. 1(c)]. Then, different from the case of single pump, the probe beam can also interact with both of the two pump beams as long as the phase matching condition is satisfied. In such dual-pump FWM interaction (as indicated by blue straight line), each pump beam annihilates one photon, the probe beam gets one photon and another photon is generated synchronously in a new conjugate beam (2). In the meantime, the new probe beam 4 (6) is generated by the single-pump interaction (yellow straight lines) between beam 2 and Pump_1 (Pump_2). In addition, the dual-pump interaction (green straight lines) between beam 3 (1) and both of the two pump beams can also generate beam 4 (6). As a result, the probe beam (5) is amplified while two new probe beams (4 and 6) and three conjugate beams (1, 2, and 3) are generated. Each process follows a double-lambda configuration as shown in Fig. 1(d). The two-dimensional intensity pattern of the output beams is shown in Fig. 1(e). Based on the interactions mentioned above, the Hamiltonian of this process can be written as

$$\hat{H} = i\hbar[\varepsilon_1\hat{a}_1^\dagger\hat{a}_5^\dagger + \varepsilon_2\hat{a}_3^\dagger\hat{a}_5^\dagger + \varepsilon_3\hat{a}_2^\dagger\hat{a}_5^\dagger + \varepsilon_4\hat{a}_2^\dagger\hat{a}_4^\dagger + \varepsilon_5\hat{a}_2^\dagger\hat{a}_6^\dagger + \varepsilon_6\hat{a}_1^\dagger\hat{a}_6^\dagger + \varepsilon_7\hat{a}_3^\dagger\hat{a}_4^\dagger] + \text{H.c.}, \quad (1)$$

where ε_i ($i = 1, 2, 3, 4, 5, 6$, and 7) denotes the interaction strength, $\hat{a}_j$ ($j = 1, 2, 3, 4, 5$, and 6) is the bosonic annihilation operator of beam j and H.c. is the Hermitian

conjugate. We find that the phases of the six generated beams and the two pump beams can be reduced to the annihilation operators. It means that the physical properties of the present SSP based FWM processes will not depend on these phases [32].

Quantum entanglement properties of Gaussian states can be completely characterized by their second-order moments, which can be conveniently organized in the form of a covariance matrix [33]. In order to obtain the covariance matrix [32], we first block the probe beam (5 in Fig. 1) via an iris, making the process purely spontaneous. Then we employ balanced homodyne detections (HDs) with local oscillators (LOs) mode matched to the six fields under interrogation to get fluctuations of amplitude $\hat{x}$ and phase $\hat{p}$ quadratures. The LOs are obtained by setting up a similar setup a few mm above the current corresponding beams [22]. Technically, much effort is made to ensure good spatial overlap between LOs and six fields under interrogation, and each HD's visibility is about 97%. Two home-made single pole six-throw switches (Switch) allow us to select any two of the photocurrents from the six HDs. Such a measurement technique of switching between pairs of modes gives the squeezing curve whose minima stay constant for repeated measurements and do not depend on which PZT is scanned. Moreover, these minima have the same value as the noise level of the absolute squeezing measurement, which has been experimentally proved using the phase locking technique before the measurements. In this way, the full covariance matrix can be reconstructed.

The entanglement of the six individual beams can be probed with the positive partial transposition (PPT) criterion, which is stated in terms of the symplectic eigenvalues of the partially transposed (PT) covariance matrix [34]. There are three kinds of possible PT operations of 1×5, 2×4, and 3×3 for hexapartite scenario, which results in 31 possible bipartitions [32]. The PPT criterion is necessary and sufficient for testing the inseparability of the bipartitions of 1×5, and sufficient for the cases of 2×4, and 3×3 [35]. Having all bipartitions not separable directly implies that all n partitions ($n > 2$) are nonseparable, meaning that the whole system is nonseparable, or fully entangled. In other words, fulfilling the PPT criterion for all possible bipartitions (i.e., all the symplectic eigenvalues are smaller than 1) is a sufficient condition to demonstrate full hexapartite entanglement [15,33,36]. In addition, the degree of entanglement can be quantified by the symplectic eigenvalues. A smaller eigenvalue implies a larger amount of entanglement.

To experimentally test the entanglement, we first set the power of the two pumps equal and then measure the covariance matrix for the cases where the pump powers are set to 26, 40, and 50 mW. As shown in Fig. 2, the overall 31 symplectic eigenvalues for each balanced pump power are all smaller than 1, which is a clear manifestation of full hexapartite entanglement. It can also be found that each

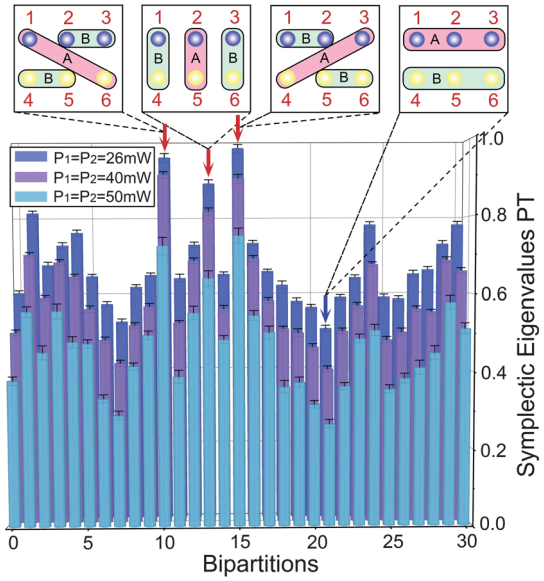

FIG. 2. Symplectic eigenvalues for all 31 bipartitions of the hexapartite states with the two balanced pump powers set to 26, 40, and 50 mW, respectively. P_1 and P_2 represent the power of $Pump_1$ and $Pump_2$. All 31 bipartitions possess an eigenvalue below 1, which indicates complete inseparability for the state. As pump power increases, the overall eigenvalues decrease monotonically, which indicates that the degree of inseparability becomes stronger. Three red arrows indicate the three largest eigenvalues while the blue one indicates the smallest eigenvalue. The corresponding bipartitions $A|B$ of 16|2345, 25|1346, 34|1256 and 123|456 are sketched sequentially on the top insets. Error bars are standard deviations.

eigenvalue decreases monotonically with the increase of pump power and the relative values of 31 symplectic eigenvalues remains almost the same. This shows that higher power of pump beams leads to stronger entanglement shared among the six output fields. This is due to the fact that the interaction between the probe and conjugate beams becomes stronger as the pump powers increase. We notice that the three largest eigenvalues labeled by red arrows in Fig. 2 for each pump power case correspond to the three scenarios $A|B$ of 16|2345, 25|1346, and 34|1256 sketched on the top insets, respectively. In other words, these three scenarios imply three weakest bipartition inseparability, showing that subsystem (1,6) is weakly entangled to the rest of the system, same for subsystems (2,5) and (3,4). Furthermore, we also notice that the smallest symplectic eigenvalue labeled by the blue arrow corresponds to the scenario $A|B$ of 123|456 also sketched on the top inset, showing the strongest bipartition inseparability and indicating that subsystem (1,2,3) is strongly entangled with the subsystem (4,5,6).

One can imagine that the system can be degraded into the normal single-pump FWM process if one of the pump beam is much weaker than the other, or is completely blocked. This shows the possibility of reconfiguring the SSP based FWM processes by regulating the power ratio of

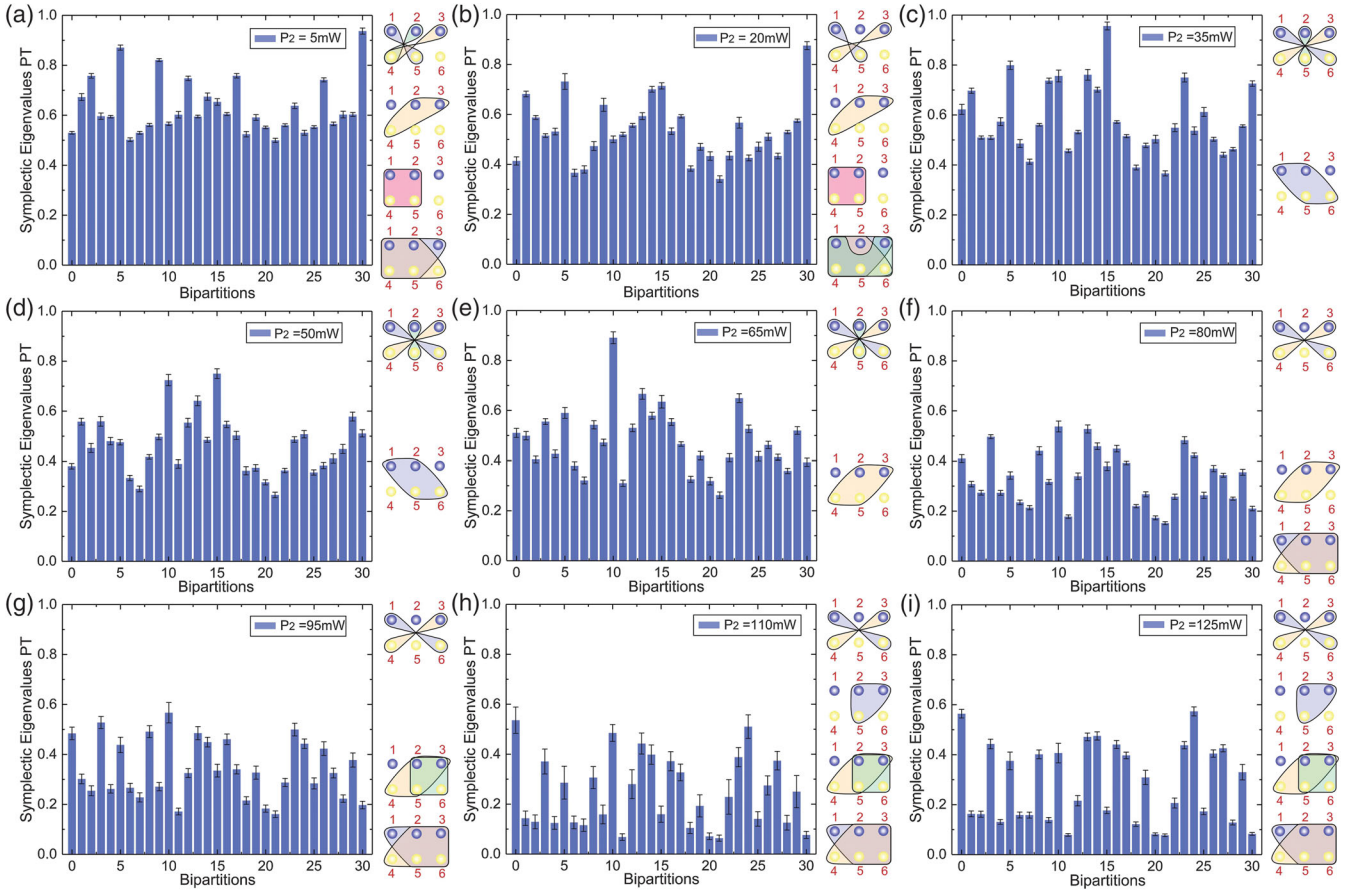

FIG. 3. Reconfiguration of the hexapartite entanglement structure through tailoring the power ratio of the two pump beams. (a)–(i) Symplectic eigenvalues when Pump_1 is kept at 50 mW and Pump_2 is set as 5, 20, 35, 50, 65, 80, 95, 110, and 125 mW, respectively. The different distribution of m-partite entanglement (with $m = 2, 3, 4, 5$) embedded within the hexapartite states for different pump power ratio are shown as the right insets of each subfigure. Such m-partite entanglement distribution can be used to characterize the entanglement structure of the hexapartite entanglement. Note that the hexapartite entanglement is present for all the cases studied in this figure.

the two pump beams. For this purpose, we have studied the hexapartite entanglement for different pump power ratios by fixing one of the pump beam as 50 mW and varying the other one from 5 to 125 mW with a step of 15 mW. The results are shown in Fig. 3, which clearly manifest the presence of full hexapartite entanglement for all the cases.

Although these eigenvalues give information on the structure of the state and how the multipartite entanglement is spread, they are not easy to interpret. To better illustrate the internal structure of the generated state and how entanglement is shared within the hexapartite entangled beams, for each pump configuration we consider any subset of m modes (with $m = 2, 3, 4, 5$) and check m-partite entanglement embedded within our hexapartite states. The results are shown in the right insets of Figs. 3(a)–3(i). It can be seen that the internal structure of the hexapartite entanglement characterized by such subsystem entanglement distribution largely depends on the pump power ratio. The more asymmetrical the pump shape is, the richer the entanglement structure will be. For example, when the two pumps have similar power [Figs. 3(c)–3(e)], the symmetry of the situation implies that there are 2-partite entanglement for subsets (1,6), (2,5), and (3,4), but neither 3-partite nor 5-partite entanglement. While when the two pumps have much different powers (other subfigures), subsets of 2-partite entanglement become different and, more importantly, 3-partite or 5-partite entanglement emerges. All these results clearly show that the internal structure of the generated hexapartite entanglement can be efficiently

TABLE I. van Loock–Furusawa criterion for hexapartite states.

Pump cases	I	II	III	IV	V
$P_1 = 50$ mW $P_2 = 110$ mW	2.69 ±0.04	3.80 ±0.03	3.67 ±0.06	3.67 ±0.02	3.02 ±0.06
$P_1 = 50$ mW $P_2 = 125$ mW	3.09 ±0.02	3.80 ±0.02	3.01 ±0.02	3.15 ±0.03	3.13 ±0.04

manipulated by tailoring the pump power ratio, i.e., pump shaping.

In addition to PPT criterion, it is also interesting to use the van Loock-Furusawa criterion [37] to study the entanglement properties of the generated hexapartite states, as this criterion can be helpful for testing whether the obtained quantum states can be used for building quantum teleportation network [7] and for cluster state assessment through nullifiers values. For hexapartite states, the van Loock–Furusawa criterion gives a set of inequalities as follows:

$$\begin{aligned}
&\mathrm{I}\colon\ \Delta^2(\hat{x}_1-\hat{x}_2)+\Delta^2(\hat{p}_1+\hat{p}_2+g_3\hat{p}_3+g_4\hat{p}_4+g_5\hat{p}_5+g_6\hat{p}_6)\geq 4,\\
&\mathrm{II}\colon\ \Delta^2(\hat{x}_2-\hat{x}_3)+\Delta^2(g_1\hat{p}_1+\hat{p}_2+\hat{p}_3+g_4\hat{p}_4+g_5\hat{p}_5+g_6\hat{p}_6)\geq 4,\\
&\mathrm{III}\colon\ \Delta^2(\hat{x}_3-\hat{x}_4)+\Delta^2(g_1\hat{p}_1+g_2\hat{p}_2+\hat{p}_3+\hat{p}_4+g_5\hat{p}_5+g_6\hat{p}_6)\geq 4,\\
&\mathrm{IV}\colon\ \Delta^2(\hat{x}_4-\hat{x}_5)+\Delta^2(g_1\hat{p}_1+g_2\hat{p}_2+g_3\hat{p}_3+\hat{p}_4+\hat{p}_5+g_6\hat{p}_6)\geq 4,\\
&\mathrm{V}\colon\ \Delta^2(\hat{x}_5-\hat{x}_6)+\Delta^2(g_1\hat{p}_1+g_2\hat{p}_2+g_3\hat{p}_3+g_4\hat{p}_4+\hat{p}_5+\hat{p}_6)\geq 4,
\end{aligned}\tag{2}$$

where the g_i ($i=1,2,3,4,5$, and 6) can be any arbitrary real number. Note that the subscript in these inequalities does not refer to the specific number of the light beam of the hexapartite entanglement mentioned above. The violation of all the five inequalities in Eq. (2) is sufficient to demonstrate genuine hexapartite entanglement. Each term in the five inequalities of the van Loock–Furusawa criterion can be derived from the covariance matrix. As shown in Table I, by choosing proper g_i to minimize the left side of the inequalities, we find that all five inequalities are violated when Pump_2 is 110 or 125 mW and Pump_1 is 50 mW. Thus for these two cases of pump powers, the generated hexapartite states can satisfy both the PPT criterion and the van Loock–Furusawa criterion.

In conclusion, we have experimentally generated and characterized CV hexapartite entangled states by exploiting seven spatially multiplexed concurrent FWM processes driven by the SSP. The generated states for all the pump power cases satisfy the PPT criterion, showing the deterministic generation of full hexapartite entanglement. In addition, we found that the generated hexapartite entanglement structure characterized by subsystem entanglement distribution can be efficiently manipulated by pump shaping, more precisely by tailoring the pump power ratio of the SSP. Such tunability makes it possible to target a desired multipartite entanglement for a specific quantum communication task. For example, such reconfigurability is especially useful for hierarchical quantum secret sharing in which entanglement structure can decisively determine the security of the quantum network. Our apparatus is highly compact. Since our hexapartite entanglement is generated from atomic vapor, our results here can be directly applied to atomic quantum memory [38–40], a key component of quantum networks. Our scheme can also be easily scalable to a larger number of modes by shaping further the structure of the SSP, for example, changing the angle between the two pump beams or shining more pump beams. Therefore our results here pave the way to generate large scale spatially separated reconfigurable multipartite entanglement for applications in quantum communication protocols by exploiting the concept of spatial multiplexing.

This work was funded by the National Natural Science Foundation of China (NSFC) (Grants No. 11874155, No. 91436211, No. 11374104, and No. 10974057), the Natural Science Foundation of Shanghai (Grant No. 17ZR1442900), the Minhang Leading Talents (Grant No. 201971), the Program of Scientific and Technological Innovation of Shanghai (Grant No. 17JC1400401), the National Basic Research Program of China (Grant No. 2016YFA0302103), the 111 project (Grant No. B12024), the Fundamental Research Funds for the Central Universities, ECNU Academic Innovation Promotion Program for Excellent Doctoral Students (YBNL TS2019-012).

K. Z. and W. W. contributed equally to this work.

*nicolas.treps@lkb.upmc.fr
†claude.fabre@lkb.upmc.fr
‡jtjing@phy.ecnu.edu.cn

[1] B. Hensen, H. Bernien, A. E. Dréau, A. Reiserer, N. Kalb, M. S. Blok, J. Ruitenberg, R. F. L. Vermeulen, R. N. Schouten, C. Abellán, W. Amaya, V. Pruneri, M. W. Mitchell, M. Markham, D. J. Twitchen, D. Elkouss, S. Wehner, T. H. Taminiau, and R. Hanson, Nature (London) **526**, 682 (2015).
[2] S. L. Braunstein and P. van Loock, Rev. Mod. Phys. **77**, 513 (2005).
[3] C. Weedbrook, S. Pirandola, R. García-Patrón, N. J. Cerf, T. C. Ralph, J. H. Shapiro, and S. Lloyd, Rev. Mod. Phys. **84**, 621 (2012).
[4] D. P. DiVincenzo, Science **270**, 255 (1995).
[5] S. Lloyd and S. L. Braunstein, Phys. Rev. Lett. **82**, 1784 (1999).
[6] J. Jing, J. Zhang, Y. Yan, F. Zhao, C. Xie, and K. Peng, Phys. Rev. Lett. **90**, 167903 (2003).

[7] H. Yonezawa, T. Aoki, and A. Furusawa, Nature (London) **431**, 430 (2004).
[8] X. Su, S. Hao, X. Deng, L.Ma, M. Wang, X. Jia, C. Xie, and K. Peng, Nat. Commun. **4**, 2828 (2013).
[9] S. Armstrong, M. Wang, R. Y. Teh, Q. Gong, Q. He, J. Janousek, H. Bachor, M. D. Reid, and P. K. Lam, Nat. Phys. **11**, 167 (2015).
[10] X. L. Wang, L. K. Chen, W. Li, H. L. Huang, C. Liu, C. Chen, Y. H. Luo, Z. E. Su, D. Wu, Z. D. Li, H. Lu, Y. Hu, X. Jiang, C. Z. Peng, L. Li, N. L. Liu, Y. A. Chen, C. Y. Lu, and J. W. Pan, Phys. Rev. Lett. **117**, 210502 (2016).
[11] D. R. Hamel, L. K. Shalm, H. Hubel, A. J. Miller, F. Marsili, V. B. Verma, R. P. Mirin, S. W. Nam, K. J. Resch, and T. Jennewein, Nat. Photonics **8**, 801 (2014).
[12] M. Pysher, Y. Miwa, R. Shahrokhshahi, R. Bloomer, and O. Pfister, Phys. Rev. Lett. **107**, 030505 (2011).
[13] M. Chen, N. C. Menicucci, and O. Pfister, Phys. Rev. Lett. **112**, 120505 (2014).
[14] J. Roslund, R. M. de Araújo, S. Jiang, C. Fabre, and N. Treps, Nat. Photonics **8**, 109 (2014).
[15] F. A. S. Barbosa, A. S. Coelho, L. F. Muñoz-Martínez, L. Ortiz-Gutiérrez, A. S. Villar, P. Nussenzveig, and M. Martinelli, Phys. Rev. Lett. **121**, 073601 (2018).
[16] S. Yokoyama, R. Ukai, S. C. Armstrong, C. Sornphiphatphong, T. Kaji, S. Suzuki, J. Yoshikawa, H. Yonezawa, N. C. Menicucci, and A. Furusawa, Nat. Photonics **7**, 982 (2013).
[17] D. Daems and N. J. Cerf, Phys. Rev. A **82**, 032303 (2010).
[18] D. Daems, F. Bernard, N. J. Cerf, and M. I. Kolobov, J. Opt. Soc. Am. B **27**, 447 (2010).
[19] D. J. Richardson, J. M. Fini, and L. E. Nelson, Nat. Photonics **7**, 354 (2013).
[20] P. J. Winzer, Nat. Photonics **8**, 345 (2014).
[21] P. Gupta, T. Horrom, B. E. Anderson, R. Glasser, and P. D. Lett, J. Mod. Opt. **63**, 185 (2016).
[22] V. Boyer, A. M. Marino, and P. D. Lett, Science **321**, 544 (2008).
[23] A. M. Marino, R. C. Pooser, V. Boyer, and P. D. Lett, Nature (London) **457**, 859 (2009).
[24] R. C. Pooser, A. M. Marino, V. Boyer, K. M. Jones, and P. D. Lett, Phys. Rev. Lett. **103**, 010501 (2009).
[25] B. J. Lawrie, P. G. Evans, and R. C. Pooser, Phys. Rev. Lett. **110**, 156802 (2013).
[26] Z. Qin, L. Cao, H. Wang, A. M. Marino, W. Zhang, and J. Jing, Phys. Rev. Lett. **113**, 023602 (2014).
[27] F. Hudelist, J. Kong, C. Liu, J. Jing, Z. Ou, and W. Zhang, Nat. Commun. **5**, 3049 (2014).
[28] H. Wang, C. Fabre, and J. Jing, Phys. Rev. A **95**, 051802(R) (2017).
[29] J. D. Swaim, E. M. Knutson, O. Danaci, and R. T. Glasser, Opt. Lett. **43**, 2716 (2018).
[30] E. M. Knutson, J. D. Swaim, S. Wyllie, and R. T. Glasser, Phys. Rev. A **98**, 013828 (2018).
[31] J. Jia, W. Du, J. F. Chen, C. H. Yuan, Z. Y. Ou, and W. Zhang, Opt. Lett. **42**, 4024 (2017).
[32] See Supplemental Material at http://link.aps.org/supplemental/10.1103/PhysRevLett.124.090501 for details.
[33] A. S. Coelho, F. A. S. Barbosa, K. N. Cassemiro, A. S. Villar, M. Martinelli, and P. Nussenzveig, Science **326**, 823 (2009).
[34] R. Simon, Phys. Rev. Lett. **84**, 2726 (2000).
[35] R. F. Werner and M. M. Wolf, Phys. Rev. Lett. **86**, 3658 (2001).
[36] J. Sperling and W. Vogel, Phys. Rev. Lett. **111**, 110503 (2013).
[37] P. van Loock and A. Furusawa, Phys. Rev. A **67**, 052315 (2003).
[38] J.-C. Lee, K.-K. Park, T.-M. Zhao, and Y.-H. Kim, Phys. Rev. Lett. **117**, 250501 (2016).
[39] T.-M. Zhao, Y. S. Ihn, and Y.-H. Kim, Phys. Rev. Lett. **122**, 123607 (2019).
[40] M. D. Lukin, Rev. Mod. Phys. **75**, 457 (2003).